

## Article

## Fluorination Effects in XPhos Gold(I) Fluorothiolates

Guillermo Moreno-Alcántar <sup>1,\*</sup>, Cristian Díaz-Rosas <sup>1</sup>, Alberto Fernández-Alarcón <sup>2,\*</sup>, Luis Turcio-García <sup>1</sup>, Marcos Flores-Álamo <sup>1</sup>, Tomás Rocha-Rinza <sup>2</sup> and Hugo Torrens <sup>1</sup>

<sup>1</sup> Facultad de Química, Universidad Nacional Autónoma de México, Circuito Escolar, Ciudad Universitaria, Coyoacán C.P. 04510, Ciudad de México, Mexico; cristiandiaz\_chem@hotmail.com (C.D.-R.); angel\_1212@hotmail.com (L.T.-G.); mfa@unam.mx (M.F.-Á.); torrens@unam.mx (H.T.)

<sup>2</sup> Instituto de Química, Universidad Nacional Autónoma de México, Circuito Exterior, Ciudad Universitaria, Coyoacán C.P. 04510, Ciudad de México, Mexico; tomasrocharinza@gmail.com

\* Correspondence: lgma@comunidad.unam.mx (G.M.-A.); al.fedza@gmail.com (A.F.-A.); Tel.: +52-55-5622-3724 (G.M.-A.)

**Abstract:** Gold phosphine derivatives such as thiolates have been recently proposed as catalysts or catalyst precursors. The relevance of the supramolecular environment on the fine-tuning of the catalytic activity on these compounds incentivizes the use of tools that are convenient to characterize in detail the non-covalent landscape of the systems. Herein, we show the molecular and supramolecular diversity caused by the changes in the fluorination pattern in a family of new XPhos goldfluorothiolate derivatives. Furthermore, we studied the supramolecular interactions around the Au centers using quantum chemical topology tools, in particular the quantum theory of atoms in molecules (QTAIM) and the non-covalent interaction index. Our results give detailed insights into the fluorination effects on the strength of intramolecular and intermolecular interactions in these systems. We have also used QTAIM delocalization indexes to define a novel hapticity indicator. Finally, we assessed the *trans* influence of the fluorothiolates on the phosphine in terms of the change in the  $\delta$  <sup>31</sup>P-NMR. These results show the feasibility of the use of fluorination in the modulation of the electronic properties of Buchwald phosphine gold(I) compounds, and thereby its potential catalytic activity.

**Keywords:** gold complexes; non-covalent interactions; fluorinated thiolates; Buchwald ligands; QTAIM



**Citation:** Moreno-Alcántar, G.; Díaz-Rosas, C.; Fernández-Alarcón, A.; Turcio-García, L.; Flores-Álamo, M.; Rocha-Rinza, T.; Torrens, H. Fluorination Effects in XPhos Gold(I) Fluorothiolates. *Inorganics* **2021**, *9*, 14. <https://doi.org/10.3390/inorganics9020014>

Academic Editors: Laura Rodríguez and João Carlos Lima

Received: 18 January 2021

Accepted: 27 January 2021

Published: 2 February 2021

**Publisher's Note:** MDPI stays neutral with regard to jurisdictional claims in published maps and institutional affiliations.



**Copyright:** © 2021 by the authors. Licensee MDPI, Basel, Switzerland. This article is an open access article distributed under the terms and conditions of the Creative Commons Attribution (CC BY) license (<https://creativecommons.org/licenses/by/4.0/>).

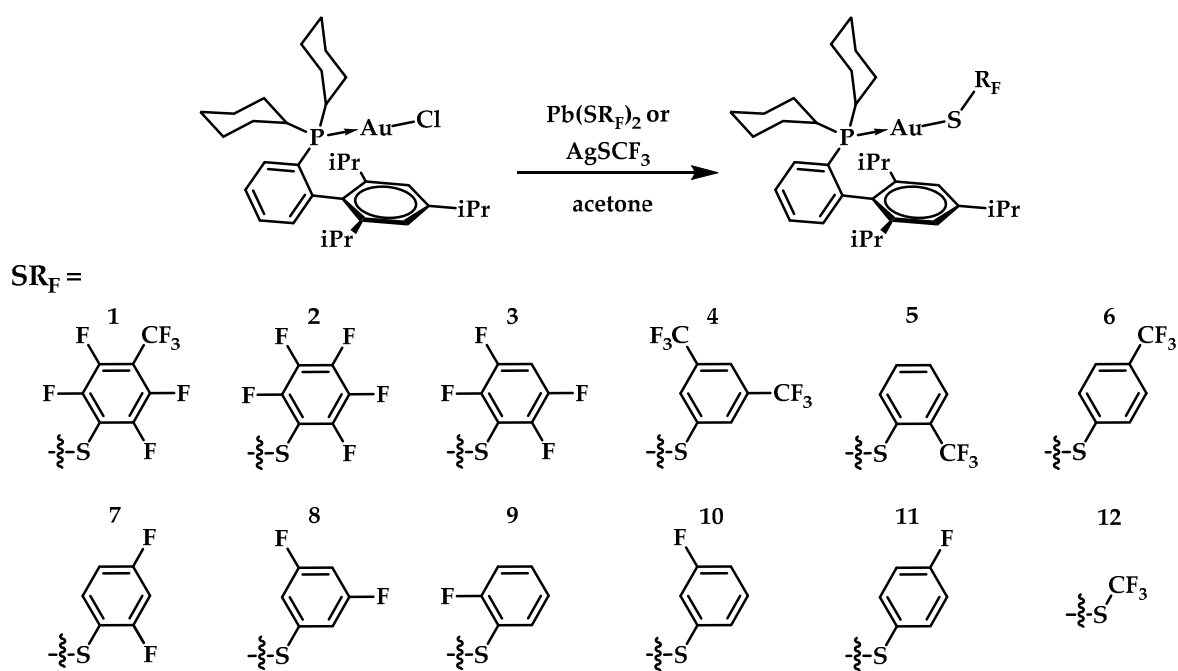
## 1. Introduction

Gold chemistry has emerged as one of the most interesting, fruitful, and promising trends in coordination and organometallic chemistry [1–3]. Taking in many cases advantage of the recurrent aurophilic interactions [4,5], gold compounds have been exploited in materials chemistry to generate light emitters [6–8], gelators [9,10], liquid crystals [11], and other self-assembled materials [12–15]. In medicinal chemistry, several gold compounds are being investigated as potentially therapeutic and theranostic agents against different diseases [16–19].

Furthermore, the catalytic activity of gold compounds has open new routes to fine chemicals of commercial relevance [20,21]. In particular, gold(I) compounds of Buchwald phosphane ligands [22] have been lately used in catalytic transformations [20,23,24]. The design of Buchwald ligands, which includes a biphenyl moiety along with other voluminous groups bonded to the donor phosphorus, delivers interesting modulation of the steric environment of the catalytic centers providing stereoselectivity to the chemical reactions [24,25]. Mechanistic studies have shown that the existence of dimeric species bridged by anionic ligands could be relevant in the output of such transformations [26]. Recently, the use as catalytic precursors of dinuclear gold complexes with bridging fluorothiolate ligands has proven successful to avoid the disadvantages of the use of silver(I) for the in-situ generation of active catalytic species [27]. Previously, fluorination has been pointed out as a strategy to provide interesting alterations to catalytic gold processes [28]. We

have recently shown that fluorination can modulate the electronic properties and the non-covalent interactions in the gold centers and their surrounding environment [29,30]. There has also been an emphasis of the potential application of such modulation in the tuning of the catalyst selectivity [31].

In this context, we have synthesized and characterized 12 new fluorinated compounds with the formula  $[\text{AuSR}_F(\text{XPhos})]$  in which  $\text{XPhos} = 2$ -dicyclohexylphosphino-2',4',6'-triisopropylbiphenyl and  $\text{SR}_F = \text{SC}_6\text{F}_4(\text{CF}_3)$ -4 (1);  $\text{SC}_6\text{F}_5$  (2);  $\text{SC}_6\text{HF}_4$ -4 (3);  $\text{SC}_6\text{H}_3(\text{CF}_3)_2$ -3,5 (4);  $\text{SC}_6\text{H}_4(\text{CF}_3)$ -2 (5);  $\text{SC}_6\text{H}_4(\text{CF}_3)$ -4 (6);  $\text{SC}_6\text{H}_3\text{F}_2$ -2,4 (7);  $\text{SC}_6\text{H}_3\text{F}_2$ -3,5 (8);  $\text{SC}_6\text{H}_4\text{F}$ -2 (9);  $\text{SC}_6\text{H}_4\text{F}$ -3 (10);  $\text{SC}_6\text{H}_4\text{F}$ -4 (11);  $\text{SCF}_3$  (12) (Scheme 1). We study the effects that fluorinated thiolate ligands exert over the gold centers in eight newly determined X-ray crystalline structures. The electronic influence of fluorination was analyzed using the quantum theory of atoms in molecules (QTAIM) applied to DFT electronic structure calculations. This methodology allowed us to study in detail both covalent and non-covalent interactions around the Au atom. The later type of contacts was also characterized using the non-covalent interaction (NCI) index. Among the most important results, we have found a relation between the Au–S bond order and the  $^{31}\text{P}$ -NMR chemical shift, indicating the *trans*-influence of the thiolates over the electronic distribution around the P atom. Particularly, our results reveal the electronic modulation exerted by the fluorinated ligands in terms of (i) the intensity of Au– $\pi$  contacts, (ii) the crystalline packing, and (iii) the *trans*-communication of the ligands. Given the importance of complexes with Buchwald ligands and thiolates in the recent development of gold catalysts, we expect these compounds to represent an attractive family of catalytic precursors with modulated activity.



**Scheme 1.** Synthetic scheme and structures of the 12  $[\text{AuSR}_F(\text{XPhos})]$  compounds presented in this work.

## 2. Results and Discussion

### 2.1. Molecular Structures

The 12 new compounds were synthesized in quantitative yields by double substitution reactions between the chlorinated precursor  $[\text{AuCl}(\text{XPhos})]$  [32,33] and the corresponding lead thiolates or  $\text{AgSCF}_3$  in the case of compound 12. Compounds 1–4, 6–8, and 12 produced suitable monocrystals for the determination of their structure by X-ray diffraction. In all these eight structures, the gold(I) center displays a nearly linear S–Au–P coordination geometry (Figure 1) with Au–P and Au–S bond distances in the usual ranges. Table 1 sum-

marizes the most important bond distances and angles observed in the studied structures. Compounds **7** and **12** display two independent molecular structures in the asymmetric unit; thus, two sets of data are displayed. In these cases, the differences between the two conformers in the crystal are small in compound **7** and more noticeable in compound **12**.

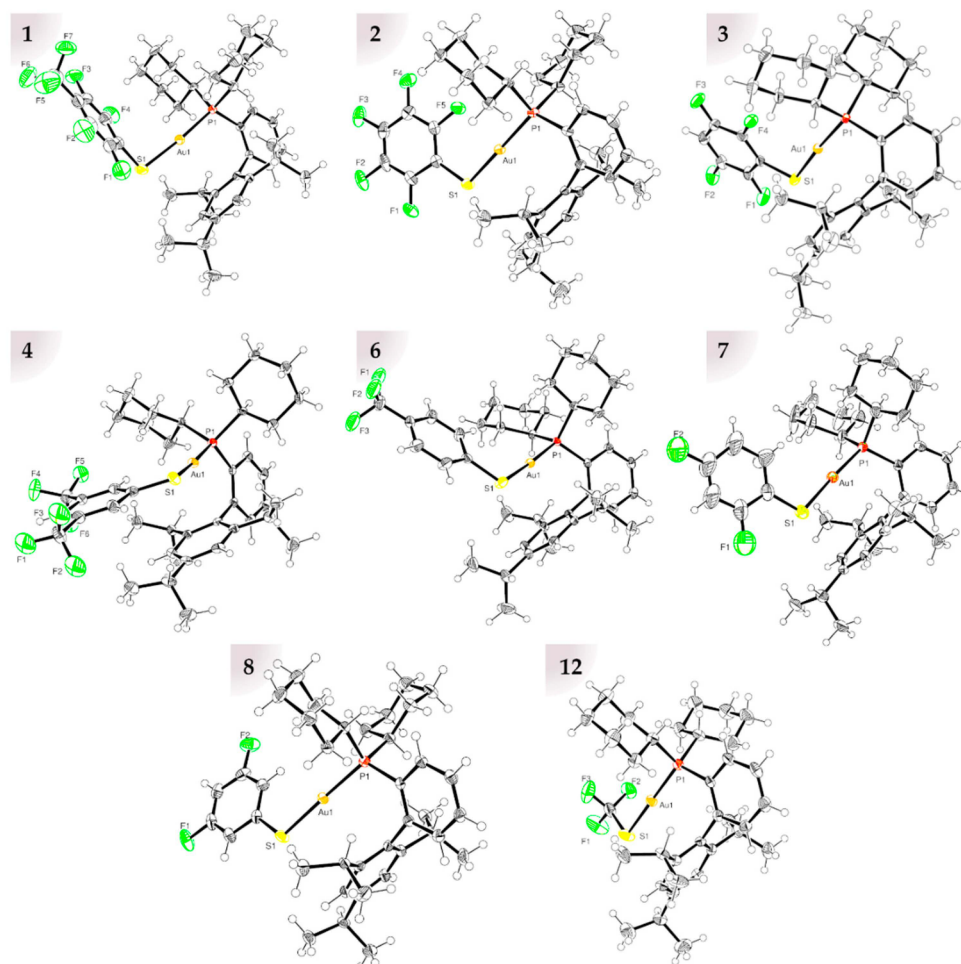


**Figure 1.** ORTEP diagrams at 50% probability level of the molecular arrangements determined by monocrystal X-ray diffraction for compounds **1–4**, **6–8**, and **12**. The conformers of **7** and **12** are shown in Figure S1.

**Table 1.** Selected distances and angles from the crystal X-ray structures of compounds **1–4**, **6–8**, and **12**. The full set of crystallographic distances and angles are available in the Supplementary Materials.

Compound	$d_{\text{Au-P}}$ (Å)	$d_{\text{Au-S}}$ (Å)	$\angle\text{P-Au-S}$ (°)	$\angle\text{Au-P-C}_{\text{Ph}}$ (°)	$\angle\text{Au-S-C}$ (°)
<b>1</b>	2.246(1)	2.297(2)	174.44(5)	115.8(2)	101.3(2)
<b>2</b>	2.261(1)	2.307(1)	177.62(3)	117.5(1)	109.0(1)
<b>3</b>	2.265(1)	2.308(1)	175.62(3)	116.3(1)	111.9(1)
<b>4</b>	2.259(1)	2.305(1)	173.25(4)	118.3(1)	106.7(2)
<b>6</b>	2.260(1)	2.298(1)	175.57(3)	117.1(1)	106.7(1)
	2.264(2)	2.313(4)	177.60(10)	115.4(3)	108.2(4)
<b>7</b>	2.262(2)	2.316(3)	176.78(9)	115.6(3)	109.9(4)
<b>8</b>	2.270(1)	2.300(1)	175.55(4)	115.4(1)	111.7(1)
	2.250(1)	2.310(2)	173.19(5)	116.0(1)	096.9(2)
<b>12</b>	2.256(1)	2.311(1)	177.42(5)	114.6(1)	101.1(2)

## 2.2. Au–Arene Contacts

The incidence of intramolecular Au–arene contacts in Buchwald-type gold complexes has attracted considerable attention [32,34–36]. To characterize these interactions within this family of compounds, we have used the Au– $\pi$  distance (i.e., the distance between the gold center and the plane generated by the capping phenyl ring). As it can be observed in Table 2, the Au– $\pi$  distances change among the series, an observation that indicates a variation in the strength of the contact as a result of the different electronic modulation caused by the fluorination of the ligand, as well as different packing effects. We have also used the hapticity ( $\eta$ ) of the Au–phenyl interaction, calculated as defined by Kochi et al. [37]. This parameter gives insights on whether the interaction involves rather the *ipso*, the *alpha*, or both carbon atoms. In the phenylthiolate derivatives, the hapticity is closer to 2, indicating a substantial contribution of the *ortho* carbon to the interaction. In contrast, compound **12** presents values closer to 1 and hence an interaction mostly formed only with the *ipso* carbon.

**Table 2.** Structural parameters determined from the crystal structures of the fluorothiolate derivatives.

Compound	Au– $\pi$ (Å)	$\eta$	Au/S/C/C (°)	$\angle\pi/\pi_F$ (°)
<b>1</b>	3.103	1.99	61.7	83.9
<b>2</b>	3.156	1.75	18.7	88.1
<b>3</b>	3.097	2.00	12.9	67.9
<b>4</b>	3.139	1.98	5.4	9.1
<b>6</b>	3.058	1.92	5.5	69.9
<b>7</b>	3.087	1.81	15.7	87.6
<b>8</b>	3.099	1.77	6.2	85.5
<b>8</b>	3.071	2.00	8.7	68.1
<b>12</b>	3.050	1.37	-	-
<b>12</b>	3.099	1.49	-	-

In order to gain further understanding into the Au– $\pi$  contacts and other non-covalent interactions occurring within the structures, we performed DFT calculations and examined the obtained electronic density by means of the QTAIM theory and the NCI-index methods of wavefunction analysis in the field of quantum chemical topology (QCT). These methods are based on the electron density  $\rho(\mathbf{r})$  and its gradient  $\nabla\rho(\mathbf{r})$ . In particular, the QTAIM, formulated by R.W. Bader [38], recovers many important chemical concepts like atoms, chemical bonds, and functional groups, among others. This theory identifies critical points of  $\rho(\mathbf{r})$  (i.e., those in which  $\nabla\rho(\mathbf{r}) = 0$ ) with nuclei (ncp), bonds (bcp), rings (rcp), and cages (ccp). On the other hand, the trajectories of  $\nabla\rho(\mathbf{r})$  are useful to describe an atom inside a molecule. There are mainly three kinds of trajectories: (i) those that come from a point in the infinity and end in an ncp, (ii) those that end in bcp and build interatomic surfaces, and (iii) those that connect two ncp, called bond paths. The union of the space delimited by the interatomic surfaces and the enclosed ncp defines an atomic basin or a topological atom. The delocalization index (DI) is a measure of the number of electrons shared between atomic basins:

$$DI(A, B) = -2\text{cov}(N_A, N_B)$$

where  $N_A$  and  $N_B$  are the electron population of the regions A and B coincident with atoms or groups of atoms. There are some developments to relate DI and the traditional concept of bond order.  $DI(A, B)$  increases with the number of electrons shared between A and B, in the same way as the bond orders [39]. In this sense, the DI could also be used to characterize the strength of non-covalent interactions.

On the other hand, the NCI index is another QCT tool that describes the non-covalent interactions in molecular or supramolecular systems. The theory subjacent to the NCI index affirms that the attractive or repulsive character of an interaction depends on the sign of the second eigenvalue ( $\lambda_2$ ) of the Hessian matrix of the electron density. Additionally, the intensity of the interactions depends on the magnitude of the electron density at the

point  $r_c$  ( $\rho(r_c)$ ) [40]. Figure 2 shows the NCI-index interaction surfaces revealed in the gold compounds addressed herein. The wrapping structure of the XPhos causes the gold atom to be embedded in a molecular cavity surrounded by diverse non-covalent contacts. In particular, the analyzed compounds show moderately attractive interactions between the gold atom and the phenyl ring, as revealed by the presence of bluish surfaces in that region. Other weak attractive intramolecular interactions recurrent in the different structures include (i)  $CH \cdots Au$  contacts that are induced by the presence of the voluminous cyclohexyl and isopropyl groups in the phosphine structure, but also formed when the thiolate fluorophenyl group presents H atoms in the position *ortho* to the sulfur; (ii)  $F \cdots Au$  interactions, especially in the 2,6 difluorinated derivatives 1–3, in which these contacts are attractive (nevertheless, although compound 7 can display this kind of interaction, the conformation showing an  $Au \cdots H$  contact is preferred); and (iii)  $S \cdots H$  and  $S \cdots \pi$  contacts promoted by the position of the thiolate along with those of the isopropyl hydrogens and the phenyl capping ring, respectively. In some cases, e.g., compounds 4, 7, and 12a, the  $S \cdots \pi$  contact is intense and contributes importantly to an extended  $(Au-S) \cdots \pi$  contact.

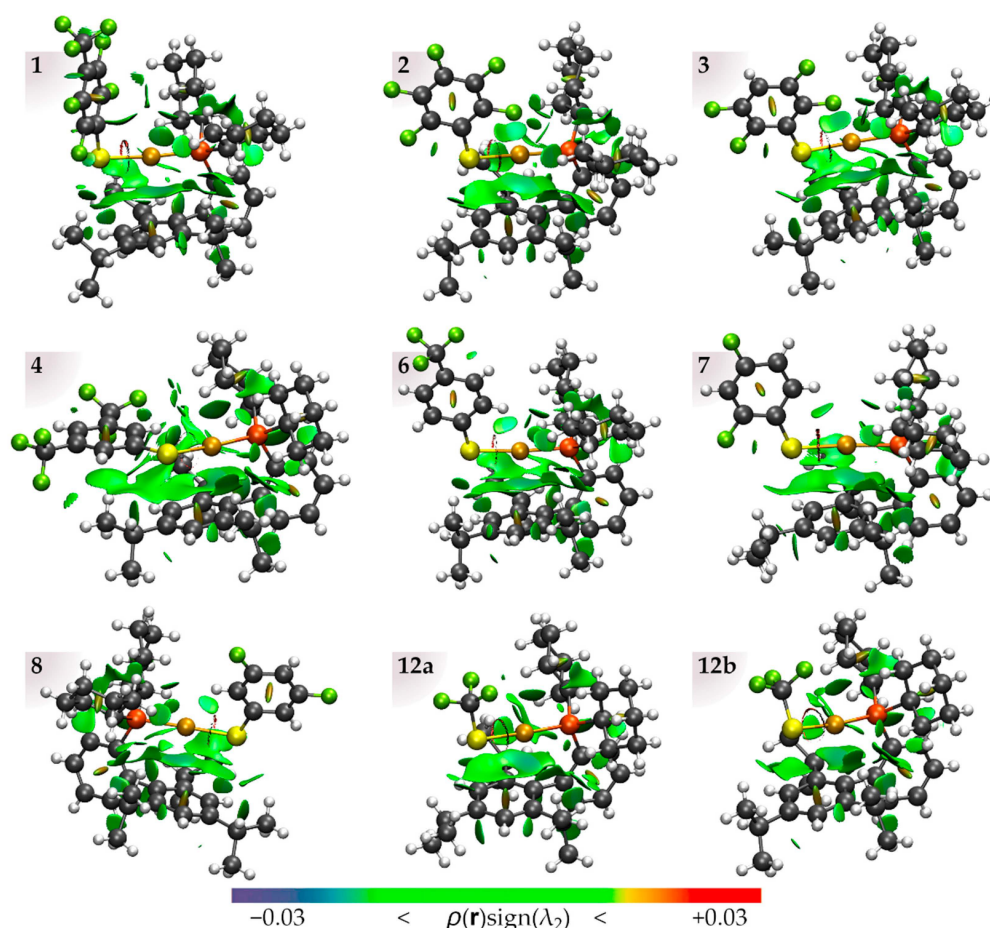


**Figure 2.** NCI-index isosurfaces revealing the intramolecular non-covalent interactions of compounds 1–4, 6–8, and 12. Due to the important differences among the two conformers of 12, both molecular arrangements were analyzed and labeled as 12a and 12b. The color code for understanding the NCI index plots is red for repulsive interactions, blue for an attractive interaction, and green for weak attractive interactions [41].

Some selected QTAIM indicators for the most relevant interactions observed in the family of compounds are listed in Table 3. The QTAIM analyses confirm important contacts existent between the Au atoms and the capping phenyl rings. In particular, all the systems show bond paths between the gold and the *ipso* carbon atom. The electron density at the

bond critical point ( $\rho(r_{\text{bcp}})$ ) and the delocalization index were used to quantify the strength of the interactions. In this regard, subtle variations of these quantities can be observed for the  $\text{Au} \cdots \text{C}_{\pi}$  among the eight analyzed compounds. In general, the larger DI and ( $\rho(r_{\text{bcp}})$ ) values show that the  $\text{Au}-\pi$  interactions strengthen as the fluorination of the thiolate ligand decreases. The distances between the gold atom and the plane generated by the  $\pi$  system for the phenylthiolate derivatives (1–4 and 6–8) correlate with the total DIs between the Au and the six carbon atoms of the phenyl ring (DI(Ph)), as shown in Figure 3a. This relation is not maintained by any of both forms of compound 12, probably due to the importantly different steric factor of the phenyl groups on the thiolate compared to the  $\text{CF}_3$ . In general, the different structure of compound 12 renders it often atypical when compared with the phenylthiolate derivatives and will therefore be further analyzed separately. As indicated by the geometrical Kochi's hapticity parameter, the  $\text{Au}-\pi$  interaction is centered in the *ipso* carbon with an important contribution of one of the *ortho* carbons. The relative contribution of each of the C atoms to the interaction, and thus the hapticity of the contact, could be also defined in terms of the relative DI magnitudes:

$$\eta_{\text{DI}} = 1 + \frac{\text{DI}(\text{Au}, \text{C}_{\text{ortho}})}{\text{DI}(\text{Au}, \text{C}_{\text{ipso}})}$$

**Table 3.** Selected  $\rho(r_{\text{bcp}})$  and DI obtained from QTAIM analyses of the electron densities in structures 1–4, 6–8, 12a, and 12b. Atomic units are used throughout.

Structure	$\rho(r_{\text{bcp}})$			DI (A,B)						$\eta_{\text{DI}}$
	Au–P	Au–S	$\text{Au} \cdots \text{C}_{\text{ipso}}$	Au, P	Au, S	Au, $\text{C}_{\text{ipso}}$	Au, $\text{C}_{\text{ortho}}$	Au, Ph	$\text{C}_{\text{ipso}}, \text{C}_{\text{ortho}}$	
1	0.125	0.110	0.016	1.017	1.031	0.082	0.077	0.244	1.284	1.94
2	0.122	0.109	0.015	1.009	1.054	0.080	0.064	0.227	1.296	1.80
3	0.121	0.108	0.016	1.007	1.047	0.084	0.076	0.238	1.293	1.90
4	0.123	0.110	0.015	1.006	1.046	0.076	0.070	0.233	1.281	1.92
6	0.122	0.112	0.017	0.998	1.070	0.084	0.084	0.263	1.277	2.00
7	0.121	0.107	0.016	1.022	1.059	0.091	0.072	0.248	1.305	1.79
8	0.120	0.110	0.017	0.998	1.082	0.088	0.080	0.249	1.288	1.90
12a	0.123	0.108	0.018	1.025	1.038	0.105	0.063	0.271	1.281	1.60
12b	0.124	0.108	0.016	1.027	1.028	0.097	0.058	0.234	1.298	1.60

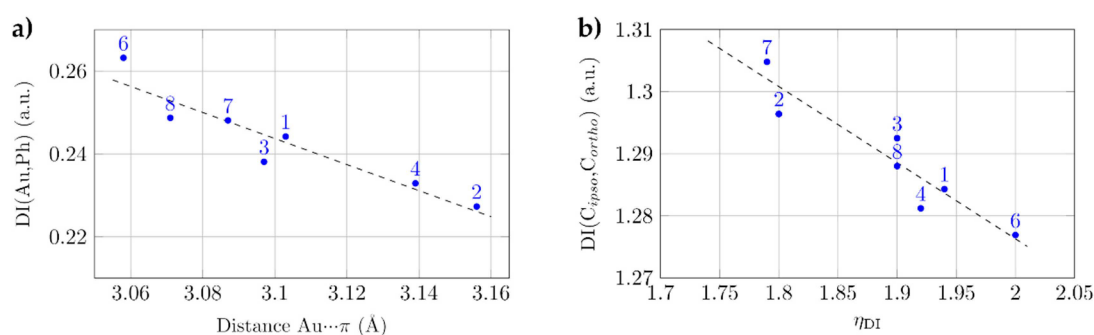


**Figure 3.** (a) Linear correlation of the distance of the gold atom to the capping phenyl ring plane ( $\text{Au} \cdots \pi$ ) with the sum of DIs of Au with the carbon atoms that comprise the phenyl ring. (b) Decrease of the DI in the  $\text{C}_{\text{ipso}}-\text{C}_{\text{ortho}}$  bond resulting from the increase in the hapticity of the  $\text{Au} \cdots \pi$  contact.

The values obtained for this DI-based hapticity of the  $\text{Au}-\pi$  interactions are presented in Table 3. Although the obtained values are generally consistent with the geometrical  $\eta$  parameter, the small differences between the two parameters are due to subtle variations in the electron density distribution that escape to the geometry examination but are revealed by the QTAIM analysis. The value of  $\eta_{\text{DI}}$  is correlated, as shown in Figure 3b, with the DI of the C–C bond involved in the interaction with gold. This observation indicates a reduction

of the bond order due to the compromise of some of the electron density associated to the C–C bond in the Au– $\pi$  contact when the hapticity is close to 2.

Compound **12** frequently diverges from the regular behavior of the family of phenylthiolate derivatives as a result of being the only aliphatic fluorothiolate derivative analyzed in this work and having different steric factors. Moreover, the X-ray crystal structure of **12** presents two significantly different molecular conformations, and the displayed differences warrant separate analysis. Both conformations show important packing effects that effectively distort their structure. Figure 2 shows the NCI analyses of the two molecular arrangements present in the asymmetric unit of the X-ray structure denoted as **12a** and **12b**. The former displays an important (Au–S)··· $\pi$  interaction that is clearly weakened in the latter arrangement. This important diminution in the intramolecular interaction is caused by the distortion of the molecule due to the compromise of the CF<sub>3</sub> group on intermolecular H-bonds, as shown in the next section. Another notable peculiarity of **12** is its lower hapticity, possibly due to the reduction of the hindrance between the thiolate and the isopropyl group that allows the P–Au–S moiety to stay centered in the XPhos molecular cavity. Although important variations are observed in the non-covalent interactions in terms of the QTAIM analyzed properties, the covalent bonds are not significantly affected by the packing differences of these conformers of **12**.

### 2.3. Crystal Packing

The introduction of fluorinated synthons into the molecular structures of the gold(I) XPhos derivatives is crucial in the crystalline packing observed in the X-ray structures of these compounds. In general, either  $\pi$ -stacking or H···F contacts drive the packing in this family of XPhos derivatives. Compounds **1**, **4**, **6**, **7**, and **12** present architectures directed by H···F contacts. Except for system **7**, all these compounds display aliphatic fluorinated groups that are known to establish strong hydrogen bonds and present contacts with either the isopropyl or cyclohexyl groups. The alternated fluorination pattern on the phenyl ring in **7** also favors the formation of H···F interactions by the increased acidity of its H atoms but shows also the contribution of S···H contacts to the supramolecular association (Figure 4).

In contrast, compounds **2**, **3**, and **8** display very similar crystal packings, characterized by the formation of  $\pi_F$ ··· $\pi_F$  interactions (Figure 5). Compound **3** shows the shorter interplanar and centroid to centroid distances among the three systems. This result is consistent with an increase of the donor–acceptor character of the interaction due to the head to tail  $\pi_F$ ··· $\pi_F$  stacking, which favors the location of the hydrogen of one molecule on top of the sulfur of the other. Further decrease of the fluorination weakens the overall strength of the interaction with a concomitant increase of the  $\pi_F$ ··· $\pi_F$  distances in compound **8**. Finally, the complete fluorinated compound **2** displays the longest distances of the group, a result that constitutes evidence of the unfavorable F···S closeness that avoids a more effective stacking.

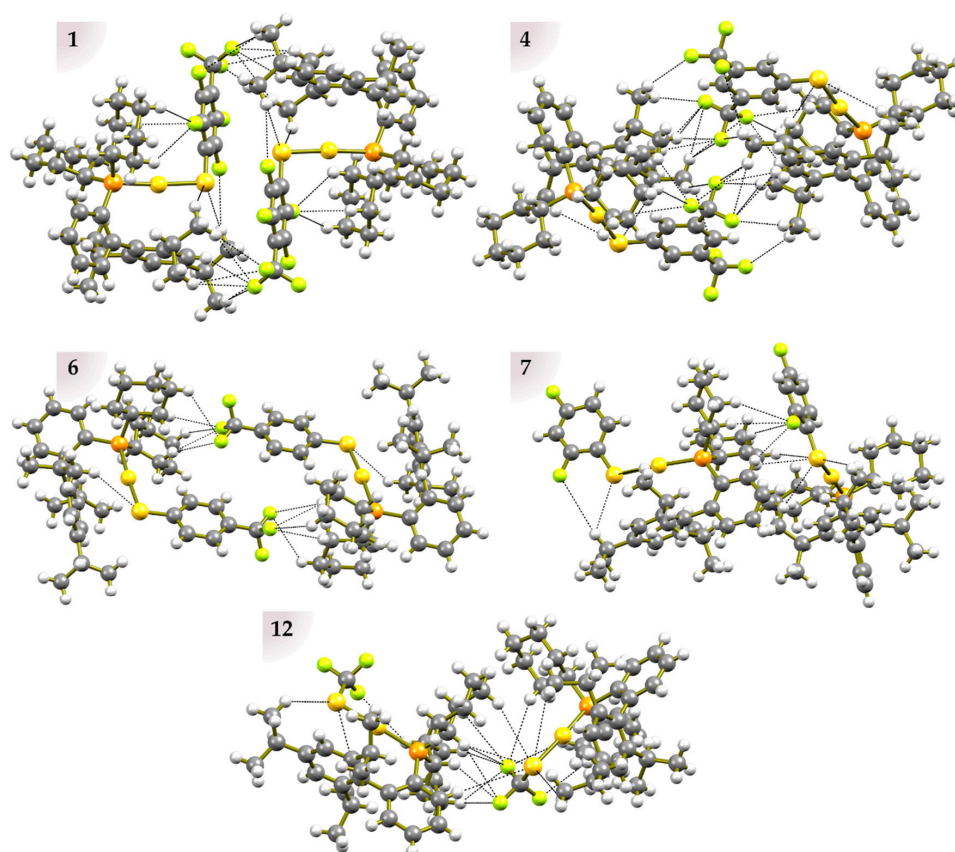


**Figure 4.** H-bond interactions ( $D-H \cdots A$ ) in the dimeric arrangements of compounds **1**, **4**, **6**, **7**, and **12**. The shown interactions present angles  $\angle_{D-H \cdots A}$  equal or greater than  $120^\circ$ , distances  $H-A$ , which differ less than  $0.5 \text{ \AA}$  with the sum of van der Waals radii [42], and at least three bonds of separation between  $D$  and  $A$  for intramolecular contacts.

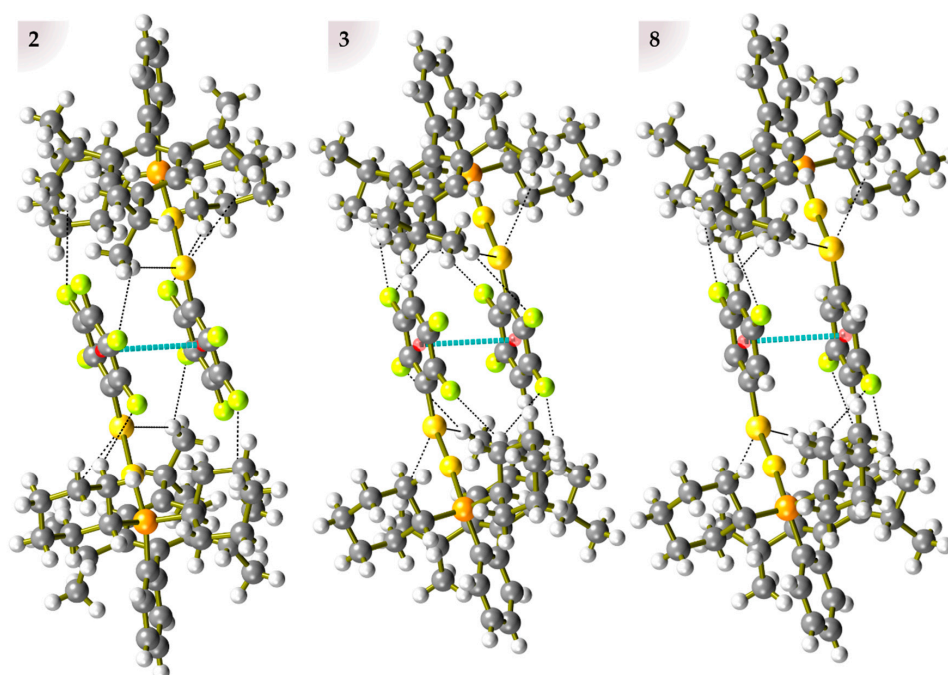


**Figure 5.** Dimeric associations of compounds **2**, **3**, and **8** displaying  $\pi_F \cdots \pi_F$  stacking interactions.  $C_6$  centroids are shown in red; the centroid-to-centroid distances (blue trace) are  $3.634$ ,  $3.490$ , and  $3.528 \text{ \AA}$ . The stacking interactions show interplanar distances of  $3.419$ ,  $3.346$ , and  $3.421 \text{ \AA}$ , respectively, for **2**, **3**, and **8**.

#### 2.4. Trans-Influence

Recently, some of us have reported the *trans*-influence [43] of fluorothiolates in linear [44] and square planar [45] metal complexes. One of the clear pieces of evidence of these influences in phosphane-gold(I) compounds relies upon the modification of the phosphorous nuclear magnetic resonance chemical shift ( $\delta^{31}\text{P-NMR}$ , Table 4). These changes occur due to the alterations in the electronic structure exerted by the *trans* thiolate via the metal center. This interplay between both ligands bonded to the metal center is characterized by the interdependency among both metal–ligand bonds. In this family of compounds, an increase in the chemical shift that indicates a deprotection of the  $^{31}\text{P}$  nucleus is related to a rise in the DIs of the Au–S bonds (Figure 6). Although the mentioned DIs are calculated for the solid-state structures, the preservation of their relationship with the NMR behavior of the compounds may point to a small disturbance of the Au–S bond by solvation effects.

**Table 4.**  $^{31}\text{P-NMR}$  chemical shifts of compounds 1–12, in chloroform-*d* solutions at 298 K.

Compound	$\delta^{31}\text{P-NMR}$ (ppm)
1	39.10
2	39.14
3	39.03
4	39.32
6	39.60
7	39.33
8	40.50
12	38.70
12b	38.70

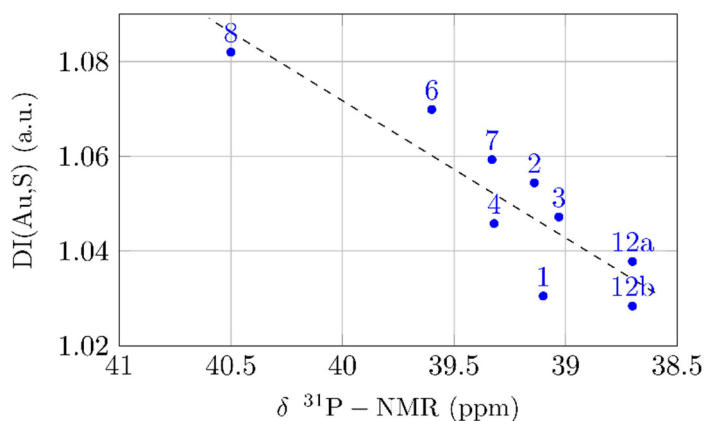


**Figure 6.** Interdependence of  $\delta^{31}\text{P-NMR}$  and the delocalization index between the Au and S atoms, which shows the influence of thiolate ligands on the electronic landscape of the *trans* phosphine ligand.

### 3. Materials and Methods

All the fluorinated thiols ( $\text{HSR}_F$ ),  $\text{Pb}(\text{CH}_3\text{COO})_2$ , and  $[\text{AuCl}(\text{XPhos})]$  were purchased from Sigma-Aldrich (St Louis, MO, USA) and used without additional treatment. Solvents were obtained from JT Baker (Thermo Fisher Scientific, Waltham, MA, USA) and used without previous treatment.  $\text{Pb}(\text{SRF})_2$  and  $\text{AgSCF}_3$  were prepared as previously reported [46,47].

ATR-FTIR spectroscopy was performed using a Perkin–Elmer Spectrum 400 (PerkinElmer, Inc., Waltham, MA, USA) in the range of 4000 to 400  $\text{cm}^{-1}$ . Elemental analysis was carried out in a Thermo Scientific Flash 200 (Thermo Fisher Scientific, Waltham, MA, USA) at 950 °C. NMR spectra were recorded on a 9.4 T Varian VNMR5 spectrometer (Varian Inc., Palo Alto, CA, USA) in  $\text{CDCl}_3$ . Chemical shifts are reported in ppm relative to the internal standard TMS  $\delta = 0$  ppm for  $^1\text{H}$  and in an 11.7 T Bruker 500 Ascend spectrometer (Bruker Co., Billerica,

MA, USA) using as external references of  $\text{CFCl}_3$  (for  $^{19}\text{F}$ ) and  $\text{H}_3\text{PO}_4$  (for  $^{31}\text{P}$ ) at 0 ppm. Positive-ion fast atom bombardment mass spectrometry (FAB+MS) spectra were measured on an MStation JMS-700 (JEOL Ltd., Tokyo, Japan).

### 3.1. Synthesis and Characterization

The 12 new compounds were synthesized by double substitution reactions from  $[\text{AuCl}(\text{XPhos})]$  with the corresponding  $\text{Pb}(\text{II})$  fluorophenylthiolate for compounds 1–11 or  $\text{AgSCF}_3$  in the case of 12. The typical synthetic procedure is exemplified by considering that of compound 1.

Compound 1,  $[\text{Au}(\text{SC}_6\text{F}_4(\text{CF}_3)_4)(\text{XPhos})]$ . In a 20 mL round bottom flask equipped with a magnetic stirrer, 120 mg (0.170 mmol) of  $[\text{AuCl}(\text{XPhos})]$  were dissolved in 5 mL of acetone. We added to this solution 60 mg (0.085 mmol) of  $\text{Pb}(\text{SC}_6\text{F}_4(\text{CF}_3)_4)_2$  suspended in 5 mL of acetone. The flask was flashed with  $\text{N}_2$ , capped, and stirred at room temperature for 24 h. Afterwards, the formed white  $\text{PbCl}_2$  was filtered and the liquid fraction concentrated at reduced pressure to a volume of ca 2 mL. Then, 10 mL of cyclohexane were added to precipitate the final product. The crude was purified by flash column chromatography using silica gel and  $\text{AcOEt}$  40:60 hexane as eluent. The product was isolated as a white powder (yield 89%). m.p. 182–185 °C; anal. 51.76, H 5.22, S 3.29 %, calcd. for  $\text{C}_{40}\text{H}_{49}\text{AuF}_7\text{PS}$ , C 52.06, H 5.35, S 3.47 %; IR (ATR)  $\nu_{\text{max}}$  2958, 2930, 2856, 1383, 1319, 1134, 1164, 999  $\text{cm}^{-1}$ ;  $^1\text{H}$  NMR (400 MHz, chloroform-*d*)  $\delta$  7.65–7.56 (m, 1H), 7.54–7.45 (m, 2H), 7.31–7.22 (m, 1H), 7.07 (s, 2H), 2.98 (hept,  $J = 6.9$  Hz, 1H), 2.24 (hept,  $J = 7.1$  Hz, 2H), 2.19–1.05 (m, 34H), 0.94 (d,  $J = 6.7$  Hz, 6H);  $^{19}\text{F}$  NMR (471 MHz, chloroform-*d*)  $\delta$  –60.61 (m), –136.82 (m), –150.54 (m);  $^{31}\text{P}$  NMR (202 MHz, chloroform-*d*) 39.10; FAB+  $m/z$  (%) 673  $[\text{XPhosAu}]^+$  (100), 922  $[\text{C}_{40}\text{H}_{48}\text{AuF}_7\text{PS}]^+$  (10), 1119  $[\text{M}+\text{Au}]^+$  (15).

Compound 2,  $[\text{Au}(\text{SC}_6\text{F}_5)(\text{XPhos})]$ . White powder, yield 93%. m.p. 193–195 °C; anal. C 53.78, H 5.44, S 3.53 %, calcd. for  $\text{C}_{39}\text{H}_{49}\text{AuF}_5\text{PS}$ , C 53.67, H 5.66, S 3.67 %; IR (ATR)  $\nu_{\text{max}}$  3054, 2958, 2927, 2853, 1383, 1122, 1002  $\text{cm}^{-1}$ ;  $^1\text{H}$  NMR (400 MHz, chloroform-*d*)  $\delta$  7.65–7.55 (m, 1H), 7.54–7.43 (m, 2H), 7.29–7.21 (m, 1H), 7.07 (s, 2H), 3.00 (hept,  $J = 6.9$  Hz, 1H), 2.25 (hept,  $J = 6.7$  Hz, 2H), 2.18–1.10 (m, 34H), 0.94 (d,  $J = 6.7$  Hz, 6H);  $^{19}\text{F}$  NMR (471 MHz, chloroform-*d*)  $\delta$  –133.45 (m), –166.95 (m), –167.29 (m);  $^{31}\text{P}$  NMR (202 MHz, chloroform-*d*) 39.14; FAB+  $m/z$  (%) 673  $[\text{XPhosAu}]^+$  (100), 872  $[\text{C}_{40}\text{H}_{48}\text{AuF}_7\text{PS}]^+$  (5), 1069  $[\text{M}+\text{Au}]^+$  (10).

Compound 3,  $[\text{Au}(\text{SC}_6\text{HF}_4)_4(\text{XPhos})]$ . White powder, yield 90%. m.p. 203–206 °C; anal. C 54.15, H 5.63, S 3.66%, calcd. for  $\text{C}_{39}\text{H}_{50}\text{AuF}_4\text{PS}$ , C 54.80, H 5.90, S 3.75 %; IR (ATR)  $\nu_{\text{max}}$  3052, 2963, 2934, 2851, 1422, 1383, 1164, 1096, 1001  $\text{cm}^{-1}$ ;  $^1\text{H}$  NMR (400 MHz, chloroform-*d*)  $\delta$  7.65–7.55 (m, 1H), 7.53–7.43 (m, 2H), 7.29–7.23 (m, 1H), 7.07 (s, 2H), 6.56 (tt,  $J = 9.9, 7.2$  Hz, 1H), 3.00 (hept,  $J = 6.8$  Hz, 1H), 2.25 (hept,  $J = 6.7$  Hz, 2H), 2.19–1.15 (m, 34H), 0.94 (d,  $J = 6.7$  Hz, 6H);  $^{19}\text{F}$  NMR (471 MHz, chloroform-*d*)  $\delta$  –132.65 (m), –142.38 (m);  $^{31}\text{P}$  NMR (202 MHz, chloroform-*d*)  $\delta$  39.03; FAB+  $m/z$  (%) 673  $[\text{XPhosAu}]^+$  (100), 854  $[\text{C}_{39}\text{H}_{49}\text{AuF}_4\text{PS}]^+$  (5), 1051  $[\text{M}+\text{Au}]^+$  (15).

Compound 4,  $[\text{Au}(\text{SC}_6\text{H}_3(\text{CF}_3)_2)_3(\text{XPhos})]$ . White powder, yield 92%. m.p. 204–206 °C (decomp.); anal. C 53.58, H 5.70, S 3.58%, calcd. for  $\text{C}_{41}\text{H}_{52}\text{AuF}_6\text{PS}$ , C 53.59, H 5.70, S 3.49%; IR (ATR)  $\nu_{\text{max}}$  3048, 2929, 2855, 1592, 1383, 1345, 1172, 765  $\text{cm}^{-1}$ ;  $^1\text{H}$  NMR (400 MHz, chloroform-*d*)  $\delta$  7.95–7.90 (m, 2H), 7.80–7.75 (m, 1H), 7.65–7.56 (m, 1H), 7.53–7.45 (m, 2H), 7.31–7.25 (m, 1H), 7.08 (s, 2H), 2.98 (hept,  $J = 6.9$  Hz, 1H), 2.24 (hept,  $J = 6.4$  Hz, 2H), 2.16–1.11 (m, 34H), 0.94 (d,  $J = 6.7$  Hz, 6H);  $^{19}\text{F}$  NMR (471 MHz, chloroform-*d*)  $\delta$  –68.20;  $^{31}\text{P}$  NMR (202 MHz, chloroform-*d*)  $\delta$  39.32; FAB+  $m/z$  (%) 673  $[\text{XPhosAu}]^+$  (100), 918  $[\text{C}_{41}\text{H}_{51}\text{AuF}_6\text{PS}]^+$  (15), 1115  $[\text{M}+\text{Au}]^+$  (18).

Compound 5,  $[\text{Au}(\text{SC}_6\text{H}_4(\text{CF}_3)_2)_2(\text{XPhos})]$ . White powder, yield 91%. m.p. 184–186 °C; anal. C 56.71, H 6.29, S 3.64%, calcd. for  $\text{C}_{40}\text{H}_{53}\text{AuF}_3\text{PS}$ , C 56.47, H 6.28, S 3.77 %; IR (ATR)  $\nu_{\text{max}}$  3058, 2926, 2854, 1461, 1436, 1381, 1124, 1030  $\text{cm}^{-1}$ ;  $^1\text{H}$  NMR (400 MHz, chloroform-*d*)  $\delta$  7.87–7.81 (m, 1H), 7.67–7.63 (m, 1H), 7.63–7.57 (m, 1H), 7.53–7.46 (m, 3H), 7.37–7.30 (m, 1H), 7.29–7.24 (m, 1H), 7.08 (s, 2H), 2.97 (hept,  $J = 7.1$  Hz, 1H), 2.24 (hept,  $J = 6.8$  Hz, 2H), 2.22–1.09 (m, 34H), 1.00–0.91 (m, 6H);  $^{19}\text{F}$  NMR (471 MHz, chloroform-*d*)  $\delta$  –62.42 (d,

$J = 2.6$  Hz);  $^{31}\text{P}$  NMR (202 MHz, chloroform-*d*)  $\delta$  39.43; FAB+  $m/z$  (%) 673 [XPhosAu] $^+$  (100), 850 [C<sub>40</sub>H<sub>52</sub>AuF<sub>3</sub>PS] $^+$  (35), 1047 [M+Au] $^+$  (10).

Compound 6, [Au(SC<sub>6</sub>H<sub>4</sub>(CF<sub>3</sub>)-4)(XPhos)]. White powder, yield 88%. m.p. 220–222 °C; anal. C 56.25, H 6.37, S 3.45%, calcd. for C<sub>40</sub>H<sub>53</sub>AuF<sub>3</sub>PS, C 56.47, H 6.28, S 3.77 %; IR (ATR)  $\nu_{\text{max}}$  3056, 2947, 2926, 2853, 1446, 1428, 1381, 1152, 1059 cm<sup>-1</sup>;  $^1\text{H}$  NMR (400 MHz, chloroform-*d*)  $\delta$  7.81–7.63 (m, 2H), 7.65–7.53 (m, 3H), 7.53–7.45 (m, 2H), 7.31–7.25 (m, 1H), 7.08 (s, 2H), 2.97 (hept,  $J = 6.9$  Hz, 1H), 2.24 (hept,  $J = 6.4$  Hz, 2H), 2.16–1.02 (m, 34H), 0.94 (d,  $J = 6.7$  Hz, 6H);  $^{19}\text{F}$  NMR (471 MHz, chloroform-*d*)  $\delta$  -61.75;  $^{31}\text{P}$  NMR (202 MHz, chloroform-*d*)  $\delta$  39.60; FAB+  $m/z$  (%) 673 [XPhosAu] $^+$  (100), 850 [C<sub>40</sub>H<sub>52</sub>AuF<sub>3</sub>PS] $^+$  (40), 1047 [M+Au] $^+$  (15).

Compound 7, [Au(SC<sub>6</sub>H<sub>3</sub>F<sub>2</sub>-2,4)(XPhos)]. White powder, yield 93%. m.p. 186–188 °C; anal. C 57.34, H 6.34, S 3.62%, calcd. for C<sub>39</sub>H<sub>52</sub>AuF<sub>2</sub>PS, C 57.21, H 6.40, S 3.92 %; IR (ATR)  $\nu_{\text{max}}$  3056, 2959, 2926, 2853, 1447, 1382, 1132, 1065, 1002 cm<sup>-1</sup>;  $^1\text{H}$  NMR (400 MHz, chloroform-*d*)  $\delta$  7.63–7.57 (m, 1H), 7.55–7.44 (m, 3H), 7.30–7.27 (m, 1H), 7.08 (s, 2H), 7.04–6.93 (m, 1H), 6.89–6.82 (m, 1H), 2.98 (hept,  $J = 6.9$  Hz, 1H), 2.24 (hept,  $J = 6.4$  Hz, 2H), 2.14–1.12 (m, 34H), 0.94 (d,  $J = 6.6$  Hz, 6H);  $^{19}\text{F}$  NMR (471 MHz, chloroform-*d*)  $\delta$  -106.20 (m), -124.03 (m);  $^{31}\text{P}$  NMR (202 MHz, chloroform-*d*)  $\delta$  39.33; FAB+  $m/z$  (%) 673 [XPhosAu] $^+$  (100), 818 [C<sub>39</sub>H<sub>51</sub>AuF<sub>2</sub>PS] $^+$  (12), 1015 [M+Au] $^+$  (40).

Compound 8, [Au(SC<sub>6</sub>H<sub>3</sub>F<sub>2</sub>-3,5)(XPhos)]. White powder, yield 86%. m.p. 177–180 °C; anal. C 57.17, H 6.39, S 3.93%, calcd. for C<sub>39</sub>H<sub>52</sub>AuF<sub>2</sub>PS, C 57.21, H 6.40, S 3.92 %; IR (ATR)  $\nu_{\text{max}}$  3055, 2955, 2926, 2851, 1446, 1382, 1175, 1081, 1006, 974 cm<sup>-1</sup>;  $^1\text{H}$  NMR (400 MHz, chloroform-*d*)  $\delta$  7.66–7.58 (m, 1H), 7.53–7.45 (m, 2H), 7.25–7.22 (m, 1H), 7.06 (s, 2H), 6.89 (dd,  $J = 9.1, 2.1$  Hz, 2H), 6.30 (tt,  $J = 9.2, 2.3$  Hz, 1H), 2.94 (hept,  $J = 6.8$  Hz, 1H), 2.26 (hept,  $J = 6.8$  Hz, 2H), 2.19–1.04 (m, 34H), 0.94 (d,  $J = 6.7$  Hz, 6H);  $^{19}\text{F}$  NMR (471 MHz, chloroform-*d*)  $\delta$  -114.48 (t,  $J = 8.8$  Hz);  $^{31}\text{P}$  NMR (202 MHz, chloroform-*d*)  $\delta$  40.50; FAB+  $m/z$  (%) 673 [XPhosAu] $^+$  (100), 818 [C<sub>39</sub>H<sub>51</sub>AuF<sub>2</sub>PS] $^+$  (10), 1015 [M+Au] $^+$  (35).

Compound 9, [Au(SC<sub>6</sub>H<sub>4</sub>F-2)(XPhos)]. White powder, yield 76%. m.p. 185–188 °C; anal. C 58.19, H 6.35, S 4.16%, calcd. for C<sub>39</sub>H<sub>53</sub>AuFPS, C 58.49, H 6.67, S 4.00 %; IR (ATR)  $\nu_{\text{max}}$  3059, 2959, 2925, 2851, 1426, 1381, 1117, 1069, 1002 cm<sup>-1</sup>;  $^1\text{H}$  NMR (400 MHz, chloroform-*d*)  $\delta$  7.65–7.58 (m, 1H), 7.53–7.43 (m, 3H), 7.28–7.23 (m, 1H), 7.07 (s, 2H), 6.91–6.78 (m, 2H), 6.78–6.72 (m, 1H), 2.96 (hept,  $J = 6.9$  Hz, 1H), 2.27 (hept,  $J = 6.7$  Hz, 2H), 2.21–1.04 (m, 34H), 0.94 (d,  $J = 6.7$  Hz, 6H);  $^{19}\text{F}$  NMR (471 MHz, chloroform-*d*)  $\delta$  -105.96 (m), -113.49 (m) (rotational isomers);  $^{31}\text{P}$  NMR (202 MHz, chloroform-*d*)  $\delta$  39.29; FAB+  $m/z$  (%) 673 [XPhosAu] $^+$  (100), 800 [C<sub>39</sub>H<sub>52</sub>AuFPS] $^+$  (5), 997 [M+Au] $^+$  (30).

Compound 10, [Au(SC<sub>6</sub>H<sub>4</sub>F-3)(XPhos)]. White powder, yield 81%. m.p. 151–154 °C; anal. C 58.21, H 6.43, S 3.94%, calcd. for C<sub>39</sub>H<sub>53</sub>AuFPS, C 58.49, H 6.67, S 4.00 %; IR (ATR)  $\nu_{\text{max}}$  2958, 2930, 2856, 1383, 1319, 1134, 1164, 999 cm<sup>-1</sup>;  $^1\text{H}$  NMR (400 MHz, chloroform-*d*)  $\delta$  7.67–7.57 (m, 1H), 7.53–7.44 (m, 2H), 7.28–7.22 (m, 1H), 7.14–7.09 (m, 2H), 7.07 (s, 2H), 6.95–6.84 (m, 1H), 6.59–6.50 (m, 1H), 2.94 (hept,  $J = 7.0$  Hz, 1H), 2.26 (hept,  $J = 6.9$  Hz, 2H), 2.20–1.03 (m, 34H), 0.94 (d,  $J = 6.7$  Hz, 6H);  $^{19}\text{F}$  NMR (471 MHz, chloroform-*d*)  $\delta$  -115.70 (m);  $^{31}\text{P}$  NMR (202 MHz, chloroform-*d*)  $\delta$  39.53; FAB+  $m/z$  (%) 673 [XPhosAu] $^+$  (100), 800 [C<sub>39</sub>H<sub>52</sub>AuFPS] $^+$  (8), 997 [M+Au] $^+$  (25).

Compound 11, [Au(SC<sub>6</sub>H<sub>4</sub>F-4)(XPhos)] White powder, yield 83%. m.p. 149–151 °C; anal. C 58.31, H 6.53, S 3.81%, calcd. for C<sub>39</sub>H<sub>53</sub>AuFPS, C 58.49, H 6.67, S 4.00 %; IR (ATR)  $\nu_{\text{max}}$  3054, 2959, 2924, 2853, 1427, 1380, 1203, 1087, 1002 cm<sup>-1</sup>;  $^1\text{H}$  NMR (400 MHz, chloroform-*d*)  $\delta$  7.66–7.56 (m, 1H), 7.54–7.43 (m, 2H), 7.34–7.17 (m, 3H), 7.06 (s, 2H), 6.73–6.62 (m, 2H), 2.95 (hept,  $J = 7.2$  Hz, 1H), 2.27 (hept,  $J = 6.6$  Hz, 2H), 2.21–1.06 (m, 34H), 0.94 (d,  $J = 6.7$  Hz, 6H);  $^{19}\text{F}$  NMR (471 MHz, chloroform-*d*)  $\delta$  -123.58 (m);  $^{31}\text{P}$  NMR (202 MHz, chloroform-*d*)  $\delta$  39.81; FAB+  $m/z$  (%) 673 [XPhosAu] $^+$  (100), 800 [C<sub>39</sub>H<sub>52</sub>AuFPS] $^+$  (5), 997 [M+Au] $^+$  (35).

Compound 12, [Au(SCF<sub>3</sub>)(XPhos)]. White powder (yield 95%). m.p. 195–197 °C; anal. C 52.66, H 6.35, S 4.27%, calcd. for C<sub>34</sub>H<sub>49</sub>AuF<sub>3</sub>PS, C 52.71, H 6.38, S 4.14 %; IR (ATR)  $\nu_{\text{max}}$  3057, 2951, 2920, 2848, 1607, 1460, 1445, 1361, 1268, 1001, 770 cm<sup>-1</sup>;  $^1\text{H}$  NMR (400 MHz, acetone-*d*<sub>6</sub>)  $\delta$  8.00–7.89 (m, 1H), 7.68–7.56 (m, 2H), 7.33–7.25 (m, 1H), 7.10 (s, 2H), 2.95 (hept,

$J = 6.6$  Hz, 1H), 2.50–2.40 (m, 2H), 2.35 (hept,  $J = 6.8$  Hz, 2H), 2.23–2.12 (m, 2H), 1.96–1.05 (m, 30H), 0.94 (d,  $J = 6.7$  Hz, 6H);  $^{19}\text{F}$  NMR (471 MHz, acetone- $d_6$ )  $\delta -19.08$  (d,  $J = 5.4$  Hz);  $^{31}\text{P}$  NMR (202 MHz, chloroform- $d$ )  $\delta 38.70$  (br); FAB+  $m/z$  (%) 673 [XPhosAu] $^+$  (100), 774 [C<sub>34</sub>H<sub>48</sub>AuF<sub>3</sub>PS] $^+$  (25), 971 [M+Au] $^+$  (40).

### 3.2. Crystal Structure Determination

All the compounds were crystallized by slow evaporation of solutions in acetone. Suitable single crystals of **1–4**, **6–8**, and **12**, were mounted on a glass fiber; then, crystallographic data were collected with an Oxford Diffraction Gemini “A” diffractometer with a CCD area detector at 130 K, with  $\lambda_{\text{MoK}\alpha} = 0.71073$  Å for all compounds, except **7**, for which we used  $\lambda_{\text{CuK}\alpha} = 1.54184$  Å. The unit cell parameters were determined with a set of three runs of 15 frames ( $1^\circ$  in  $\omega$ ). The double-pass method of scanning was used to exclude any noise [48]. The collected frames were integrated by using an orientation matrix determined from the narrower frame scans. Final cell constants were determined by a global refinement. Collected data were adjusted for absorbance by applying an analytical numeric absorption correction using a multifaceted crystal model based on expressions upon the Laue symmetry with equivalent reflections [49]. Structures’ solutions and refinement were carried out with the SHELXT-2014 [50] and SHELXL-2014 [51] packages. The WinGX v2020.1 [52] software was used to prepare material for publication. Full-matrix least-squares refinement was carried out by minimizing  $(F_o^2 - F_c^2)^2$ . All non-hydrogen atoms were refined anisotropically. H atoms attached to C atoms were placed in geometrically idealized positions and refined as riding on their parent atoms, with C–H = 0.98–1.00 Å and with  $U_{\text{iso}}(\text{H}) = 1.2U_{\text{eq}}(\text{C})$  for aromatic, methine, and methylene groups, and  $1.5U_{\text{eq}}(\text{C})$  for methyl groups. In compound **4**, the atoms F1, F2, and F3, and F1a, F2a, and F3a are disordered over two sites with occupancies 0.54:0.46. In compound **6**, F1, F2, F3, and F1a, F2a, F3a are disordered over two sites with occupancies 0.72:0.28. On the other hand, compound **7** presents disorder in C14b, C15b, C16b, C17b, and C18b and C14p, C15p, C16p, C17p, and C18p over two sites with occupancies 0.78:0.22, while C7b, C8b, C9b, C10b, C11b, and C12b and C7p, C8p, C9p, C10p, C11p, and C12p are disordered over two sites with occupancies 0.63:0.37. Finally, in compound **12**, the atoms C7b, C8b, C9b, and C12b and C7p, C8p, C9p, and C12p are disordered over two sites with occupancies 0.66:0.34. Crystallographic data for all complexes are presented in Tables S5–S42. Figures 4 and 5 were prepared using Mercury program [53]. The crystallographic data for the structure reported in this paper has been deposited in the Cambridge Crystallographic Data Centre as supplementary publication no. CCDC 2055607–2055614. Copies of the data can be obtained free of charge on application to CCDC, 12 Union Road, Cambridge, CB2 1EZ, UK (fax: (+44)-1223-336-033, e-mail: deposit@ccdc.cam.ac.uk).

### 3.3. Computational Details

The quantum chemical topology analyses of QTAIM were performed in the AIMAll program [54]. Electron densities were computed with the Orca [55,56] package from the experimental X-ray structures with the BP086 functional [57,58] along with def2-TZVP basis set [59] and the Zeroth Order Regular Approximation (ZORA) [60] in order to get a good description of relativistic effects in gold atoms [61]. The NCI isosurfaces were obtained with NCIPLOT [41] and visualized in the VMD program [62].

## 4. Conclusions

The modification of the fluorination pattern into this series of thiolate gold(I) derivatives including the Buchwald phosphine XPhos has shown to exert a substantial modulation over the type and intensity of the *intra*- and *inter*-molecular non-covalent interactions formed by these compounds. This modulation is due to (i) the introduction of new synthons that direct the supramolecular crystal packing and (ii) the electronic modifications that determine the molecular conformations. The theoretical and topological study of the crystallographic structures, via the QTAIM and the NCI-index, allowed us to characterize

the properties of the studied systems in a more comprehensive way than that based on a sole geometrical analysis. In particular, we proposed a DI-based indicator for the hapticity of the M- $\pi$  contacts ( $\eta_{DI}$ ), which comprises subtle electronic disturbances not contemplated in the geometrical hapticity. Finally, we have observed the existence of electronic *trans*-communication among the thiolate and phosphine ligands, as revealed by the direct relation of the  $^{31}\text{P}$  NMR chemical shift with the DI(Au,S). This result provides evidence of the change in the thiolate *trans*-influence due to fluorination. This kind of electronic modulation could be helpful in the fine tuning of the catalytic activity of gold(I) compounds, opening new paths in the design of Au derivatives bearing thiolate and phosphine ligands.

**Supplementary Materials:** The following are available online at <https://www.mdpi.com/2304-6740/9/2/14/s1>: Supplementary figures, regression parameters for the plots in Figures 3 and 6, Crystallographic tables, CIF and checkCIF files.

**Author Contributions:** Conceptualization: H.T., and G.M.-A.; methodology: G.M.-A., H.T., and A.F.-A.; experimentation: G.M.-A., C.D.-R., and L.T.-G.; X-ray experiments: M.F.-Á.; computational study: A.F.-A. and T.R.-R.; formal analysis: G.M.-A.; writing—original draft preparation: G.M.-A. and A.F.-A.; writing—review and editing: H.T. and T.R.-R.; supervision: H.T., T.R.-R., and G.M.-A.; project administration: H.T., T.R.-R., and G.M.-A.; funding acquisition: H.T., and T.R.-R. All authors have read and agreed to the published version of the manuscript.

**Funding:** This research was funded by DGAPA-UNAM grant IN210818, and CONACYT-Mexico project CB-2012/177498, and postdoctoral grant 740732.

**Acknowledgments:** We acknowledge the instrumental support of the Unit for Industry and Research Support (USAI) at the School of Chemistry of UNAM, Mexico. The authors are also thankful for the DGTIC/UNAM project LANCAD-DGTIC-UNAM-250 for computer time. We thank Laura Rodriguez and João Carlos Lima for the kind invitation to submit this work.

**Conflicts of Interest:** The authors declare no conflict of interest.

## References

1. Puddephatt, R.J. *The Chemistry of Gold, Topics in Inorganic and General Chemistry*; Elsevier Scientific Pub. Co.: Amsterdam, The Netherlands, 1978.
2. Sadler, P.J. Gold chemistry. *Gold Bull.* **2009**, *42*, 220. [[CrossRef](#)]
3. Schmidbaur, H. The fascinating implications of new results in gold chemistry. *Gold Bull.* **1990**, *23*, 11–21. [[CrossRef](#)]
4. Schmidbaur, H.; Schier, A. Auophilic interactions as a subject of current research: An up-date. *Chem. Soc. Rev.* **2012**, *41*, 370–412. [[CrossRef](#)] [[PubMed](#)]
5. Tiekink, E.R.T. Supramolecular assembly based on “emerging” intermolecular interactions of particular interest to coordination chemists. *Co-ord. Chem. Rev.* **2017**, *345*, 209–228. [[CrossRef](#)]
6. He, X.; Yam, V.W.-W. Luminescent gold(I) complexes for chemosensing. *Coord. Chem. Rev.* **2011**, *255*, 2111–2123. [[CrossRef](#)]
7. Lima, J.C.; Rodríguez, L. Highlights on gold TADF complexes. *Inorganics* **2019**, *7*, 124. [[CrossRef](#)]
8. Langdon-Jones, E.E.; Pope, S.J.A. Recent developments in gold(I) coordination chemistry: Luminescence properties and bioimaging opportunities. *Chem. Commun.* **2014**, *50*, 10343–10354. [[CrossRef](#)]
9. Lima, J.; Rodríguez, L.; Lima, J.C.; Rodríguez, L. Supramolecular gold metallogelators: The key role of metallophilic interactions. *Inorganics* **2014**, *3*, 1–18. [[CrossRef](#)]
10. Blasco, D.; López-De-Luzuriaga, J.M.; Monge, M.; Olmos, M.E.; Pascual, D.; Rodríguez-Castillo, M. Cooperative Au(I)···Au(I) interactions and hydrogen bonding as origin of a luminescent adeninate hydrogel formed by ultrathin molecular nanowires. *Inorg. Chem.* **2018**, *57*, 3805–3817. [[CrossRef](#)]
11. Bardají, M. Gold liquid crystals in the XXI century. *Inorganics* **2014**, *2*, 433–454. [[CrossRef](#)]
12. Kui, S.C.F.; Huang, J.-S.; Sun, R.W.-Y.; Zhu, N.; Che, C.-M. Self-assembly of a highly stable, topologically interesting metalla-macrocyclic by bridging gold(I) ions with pyridyl-2,6-diphenyl- and diphosphanes. *Angew. Chem. Int. Ed.* **2006**, *45*, 4663–4666. [[CrossRef](#)] [[PubMed](#)]
13. Aguiló, E.; Moro, A.J.; Gavara, R.; Alfonso, I.; Pérez, Y.; Zaccaria, F.; Guerra, C.F.; Malfois, M.; Baucells, C.; Ferrer, M.; et al. Reversible self-assembly of water-soluble gold(I) complexes. *Inorg. Chem.* **2018**, *57*, 1017–1028. [[CrossRef](#)] [[PubMed](#)]
14. Wu, Z.; Du, Y.; Liu, J.; Yao, Q.; Chen, T.; Cao, Y.; Zhang, H.; Xie, J. Auophilic interactions in the self-assembly of gold nanoclusters into nanoribbons with enhanced luminescence. *Angew. Chem. Int. Ed.* **2019**, *58*, 8139–8144. [[CrossRef](#)] [[PubMed](#)]
15. Shakirova, J.R.; Grachova, E.V.; Karttunen, A.J.; Gurzhiy, V.V.; Tunik, S.P.; Koshevoy, I.O. Metallophilicity-assisted assembly of phosphine-based cage molecules. *Dalton Trans.* **2014**, *43*, 6236. [[CrossRef](#)] [[PubMed](#)]
16. Ott, I. On the medicinal chemistry of gold complexes as anticancer drugs. *Coord. Chem. Rev.* **2009**, *253*, 1670–1681. [[CrossRef](#)]

17. Bertrand, B.; Casini, A. A golden future in medicinal inorganic chemistry: The promise of anticancer gold organometallic compounds. *Dalton Trans.* **2014**, *43*, 4209–4219. [[CrossRef](#)]
18. Zou, T.; Lum, C.T.; Lok, C.-N.; Zhang, J.-J.; Che, C.-M. Chemical biology of anticancer gold(III) and gold(I) complexes. *Chem. Soc. Rev.* **2015**, *44*, 8786–8801. [[CrossRef](#)]
19. Pang, B.; Yang, X.; Xia, Y. Putting gold nanocages to work for optical imaging, controlled release and cancer theranostics. *Nanomedicine* **2016**, *11*, 1715–1728. [[CrossRef](#)]
20. Echavarren, A.M.; Hashmi, A.S.K.; Toste, F.D. Gold catalysis—steadily increasing in importance. *Adv. Synth. Catal.* **2016**, *358*, 1347. [[CrossRef](#)]
21. Ciriminna, R.; Falletta, E.; Della Pina, C.; Teles, J.H.; Pagliaro, M. Industrial applications of gold catalysis. *Angew. Chem. Int. Ed.* **2016**, *55*, 14210–14217. [[CrossRef](#)]
22. Barder, T.E.; Buchwald, S.L. Rationale behind the resistance of dialkylbiaryl phosphines toward oxidation by molecular oxygen. *J. Am. Chem. Soc.* **2007**, *129*, 5096–5101. [[CrossRef](#)] [[PubMed](#)]
23. Zuccarello, G.; Zanini, M.; Echavarren, A.M. Buchwald-type ligands on gold(I) catalysis. *Isr. J. Chem.* **2020**, *60*, 360–372. [[CrossRef](#)]
24. Surry, D.S.; Buchwald, S.L. Biaryl phosphane ligands in palladium-catalyzed amination. *Angew. Chem. Int. Ed.* **2008**, *47*, 6338–6361. [[CrossRef](#)] [[PubMed](#)]
25. Billingsley, K.; Buchwald, S.L. Highly Efficient Monophosphine-Based Catalyst for the Palladium-Catalyzed Suzuki–Miyaura reaction of heteroaryl halides and heteroaryl boronic acids and esters. *J. Am. Chem. Soc.* **2007**, *129*, 3358–3366. [[CrossRef](#)]
26. Homs, A.; Escofet, I.; Echavarren, A.M. On the silver effect and the formation of chloride-bridged digold complexes. *Org. Lett.* **2013**, *15*, 5782–5785. [[CrossRef](#)]
27. Visbal, R.; Herrera, R.P.; Gimeno, M.C. Thiolate bridged gold(I)–NHC catalysts: New approach for catalyst design and its application to trapping catalytic intermediates. *Chem. A Eur. J.* **2019**, *25*, 15837–15845. [[CrossRef](#)]
28. Miró, J.; Del Pozo, C. Fluorine and gold: A fruitful partnership. *Chem. Rev.* **2016**, *116*, 11924–11966. [[CrossRef](#)]
29. Moreno-Alcantar, G.; Turcio-García, L.; Guevara-Vela, J.M.; Romero-Montalvo, E.; Rocha-Rinza, T.; Pendás, Á.M.; Flores-Álamo, M.; Torrens, H. Directing the crystal packing in triphenylphosphine gold(I) thiolates by ligand fluorination. *Inorg. Chem.* **2020**, *59*, 8667–8677. [[CrossRef](#)]
30. Moreno-Alcantar, G.; Guevara-Vela, J.M.; Delgadillo-Ruiz, R.; Rocha-Rinza, T.; Martín Pendás, Á.; Flores-Álamo, M.; Torrens, H. Structural effects of trifluoromethylation and fluorination in gold(I) BIPHEP fluorothiolates. *New J. Chem.* **2017**, *41*, 10537–10541. [[CrossRef](#)]
31. Cordón, J.; Jiménez-Osés, G.; López-De-Luzuriaga, J.M.; Monge, M. The key role of Au-substrate interactions in catalytic gold subnanoclusters. *Nat. Commun.* **2017**, *8*, 1657. [[CrossRef](#)]
32. Partyka, D.V.; Robilotto, T.J.; Zeller, M.; Hunter, A.D.; Gray, T.G. Dialkylbiarylphosphine complexes of gold(I) halides. Gold–aryl  $\pi$ -interactions in the solid state. *Organometallics* **2008**, *27*, 28–32. [[CrossRef](#)]
33. Nieto-Oberhuber, C.; López, S.; Echavarren, A.M. Intramolecular [4 + 2] cycloadditions of 1,3-enynes or arylalkynes with alkenes with highly reactive cationic phosphine Au(I) complexes. *J. Am. Chem. Soc.* **2005**, *127*, 6178–6179. [[CrossRef](#)] [[PubMed](#)]
34. Pérez-Galán, P.; Delpont, N.; Herrero-Gómez, E.; Maseras, F.; Echavarren, A.M. Metal-arene interactions in dialkylbiarylphosphane complexes of copper, silver, and gold. *Chem. A Eur. J.* **2010**, *16*, 5324–5332. [[CrossRef](#)] [[PubMed](#)]
35. Herrero-Gómez, E.; Nieto-Oberhuber, C.; López, S.; Benet-Buchholz, J.; Echavarren, A.M. Cationic  $\eta^1/\eta^2$ -Gold(I) complexes of simple arenes. *Angew. Chem. Int. Ed.* **2006**, *45*, 5455–5459. [[CrossRef](#)] [[PubMed](#)]
36. Moreno-Alcantar, G.; Hess, K.; Guevara-Vela, J.M.; Rocha-Rinza, T.; Martín Pendás, Á.; Flores-Álamo, M.; Torrens, H.  $\pi$ -backbonding and non-covalent interactions in the JohnPhos and polyfluorothiolate complexes of gold(i). *Dalton Trans.* **2017**, *46*, 12456–12465. [[CrossRef](#)] [[PubMed](#)]
37. Vasilyev, A.V.; Lindeman, S.V.; Kochi, J.K. Noncovalent binding of the halogens to aromatic donors. Discrete structures of labile Br<sub>2</sub> complexes with benzene and toluene. *Chem. Commun.* **2001**, 909–910. [[CrossRef](#)]
38. Bader, R.F.W. *Atoms in Molecules: A Quantum Theory*; Clarendon Press: Oxford, UK, 1990; ISBN 0198558651.
39. Fradera, X.; Austen, M.A.; Bader, R.F.W. The Lewis Model and beyond. *J. Phys. Chem. A* **1999**, *103*, 304–314. [[CrossRef](#)]
40. Johnson, E.R.; Keinan, S.; Mori-Sánchez, P.; Contreras-García, J.; Cohen, A.J.; Yang, W. Revealing noncovalent interactions. *J. Am. Chem. Soc.* **2010**, *132*, 6498–6506. [[CrossRef](#)]
41. Contreras-García, J.; Johnson, E.R.; Keinan, S.; Chaudret, R.; Piquemal, J.-P.; Beratan, D.N.; Yang, W. NCIPLOT: A program for plotting noncovalent interaction regions. *J. Chem. Theory Comput.* **2011**, *7*, 625–632. [[CrossRef](#)]
42. Bondi, A. van der Waals Volumes and Radii. *J. Phys. Chem.* **1964**, *68*, 441–451. [[CrossRef](#)]
43. Appleton, T.; Clark, H.; Manzer, L. The trans-influence: Its measurement and significance. *Coord. Chem. Rev.* **1973**, *10*, 335–422. [[CrossRef](#)]
44. Moreno-Alcantar, G.; Hernández-Toledo, H.; Guevara-Vela, J.M.; Rinza, T.R.; Pendás, Á.M.; Flores-Álamo, M.; Torrens, H. Stability and trans influence in fluorinated gold(I) coordination compounds. *Eur. J. Inorg. Chem.* **2018**, *2018*, 4413–4420. [[CrossRef](#)]
45. Cervantes, R.; Tiburcio, J.; Torrens, H. Cis and trans influences on [Pt(SR F)(triphos)] + complexes (SR F = polyfluorobenzothiolate). *New J. Chem.* **2014**, *39*, 631–638. [[CrossRef](#)]
46. Moreno-Alcantar, G.; Salazar, L.; Romo-Islands, G.; Flores-Álamo, M.; Torrens, H. Exploring the self-assembled tacticity in aurophilic polymeric arrangements of diphosphanegold(I) fluorothiolates. *Molecules* **2019**, *24*, 4422. [[CrossRef](#)] [[PubMed](#)]

47. Biggs, A.I.; Baddiley, J.; Hughes, N.A.; Mehra, H.S.; Trotman-Dickenson, A.F.; Verbeke, G.J.O.; Barraclough, C.C.; Nyholm, R.S.; Beattie, I.R.; Gilson, T.; et al. Notes. *J. Chem. Soc.* **1961**, 2572–2600. [[CrossRef](#)]
48. Agilent. *CrysAlis PRO*; Agilent Technologies Ltd.: Yarnton, UK, 2014.
49. Clark, R.C.; Reid, J.S. The analytical calculation of absorption in multifaceted crystals. *Acta Crystallogr. Sect. A Found. Crystallogr.* **1995**, *51*, 887–897. [[CrossRef](#)]
50. Sheldrick, G.M. SHELXT—Integrated space-group and crystal-structure determination. *Acta Crystallogr. Sect. A Found. Adv.* **2015**, *71*, 3–8. [[CrossRef](#)]
51. Sheldrick, G.M. Crystal structure refinement with SHELXL. *Acta Crystallogr. Sect. C Struct. Chem.* **2015**, *71*, 3–8. [[CrossRef](#)]
52. Farrugia, L.J. WinGXandORTEP for Windows: An update. *J. Appl. Crystallogr.* **2012**, *45*, 849–854. [[CrossRef](#)]
53. Macrae, C.F.; Sovago, I.; Cottrell, S.J.; Galek, P.T.A.; McCabe, P.; Pidcock, E.; Platings, M.; Shields, G.P.; Stevens, J.S.; Towler, M.; et al. Mercury 4.0: From visualization to analysis, design and prediction. *J. Appl. Crystallogr.* **2020**, *53*, 226–235. [[CrossRef](#)]
54. Keith, T.A. *AIMAll 2019*, version 19.10.12; Gristmill Software: Overland Park, KS, USA, 2019.
55. Neese, F. The ORCA program system. *Wiley Interdiscip. Rev. Comput. Mol. Sci.* **2012**, *2*, 73–78. [[CrossRef](#)]
56. Neese, F. Software update: The ORCA program system, version 4.0. *Wiley Interdiscip. Rev. Comput. Mol. Sci.* **2017**, *e8*, 1327. [[CrossRef](#)]
57. Levy, M.; Perdew, J.P. Success of quantum mechanical approximations for molecular geometries and electron–nuclear attraction expectation values: Gift of the Coulomb potential? *J. Chem. Phys.* **1986**, *84*, 4519–4523. [[CrossRef](#)]
58. Becke, A.D. Density-functional exchange-energy approximation with correct asymptotic behavior. *Phys. Rev. A* **1988**, *38*, 3098–3100. [[CrossRef](#)]
59. Pantazis, D.A.; Chen, X.-Y.; Landis, C.R.; Neese, F. All-Electron Scalar Relativistic Basis Sets for Third-Row Transition Metal Atoms. *J. Chem. Theory Comput.* **2008**, *4*, 908–919. [[CrossRef](#)]
60. Van Lenthe, E.; Baerends, E.J.; Snijders, J.G. Relativistic regular two-component Hamiltonians. *J. Chem. Phys.* **1993**, *99*, 4597–4610. [[CrossRef](#)]
61. van Wüllen, C. Molecular density functional calculations in the regular relativistic approximation: Method, application to coinage metal diatomics, hydrides, fluorides and chlorides, and comparison with first-order relativistic calculations. *J. Chem. Phys.* **1998**, *109*, 392–399. [[CrossRef](#)]
62. Humphrey, W.; Dalke, A.; Schulten, K. VMD: Visual molecular dynamics. *J. Mol. Graph.* **1996**, *14*, 33–38. [[CrossRef](#)]